

# ScholarWorks@GSU

## Structures of Darunavir-Resistant HIV#1 Protease Mutant Reveal Atypical Binding of Darunavir to Wide Open Flaps

Authors	Zhang, Ying;Chang, Yu-Chung E.;Louis, John M.;Wang, Yuan Fang;Harrison, Robert W.;Weber, Irene
Citation	Ying Zhang, Yu-Chung E. Chang, John M. Louis, Yuan-Fang Wang, Robert W. Harrison, and Irene T. Weber. Structures of Darunavir-Resistant HIV-1 Protease Mutant Reveal Atypical Binding of Darunavir to Wide Open Flaps. ACS Chemical Biology 2014 9 (6), 1351-1358. doi: <a href="http://dx.doi.org/10.1021/cb4008875">http://dx.doi.org/10.1021/cb4008875</a>
Download date	2026-05-20 04:52:25
Link to Item	<a href="https://hdl.handle.net/20.500.14694/2882">https://hdl.handle.net/20.500.14694/2882</a>

# Structures of Darunavir-Resistant HIV-1 Protease Mutant Reveal Atypical Binding of Darunavir to Wide Open Flaps

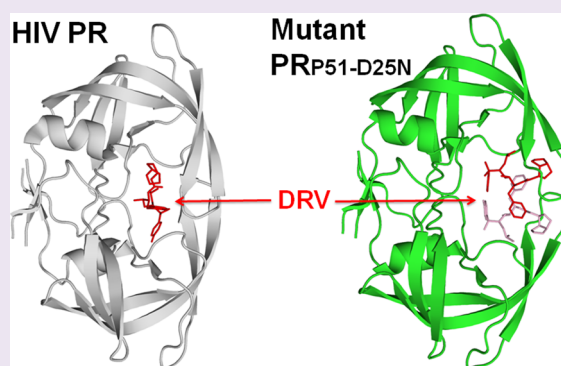
Ying Zhang,<sup>†</sup> Yu-Chung E. Chang,<sup>‡,⊥</sup> John M. Louis,<sup>||</sup> Yuan-Fang Wang,<sup>‡</sup> Robert W. Harrison,<sup>‡,§</sup> and Irene T. Weber<sup>\*,†,‡</sup>

<sup>†</sup>Department of Chemistry, <sup>‡</sup>Department of Biology, and <sup>§</sup>Department of Computer Science, Georgia State University, Atlanta, Georgia 30303, United States

<sup>||</sup>Laboratory of Chemical Physics, National Institute of Diabetes and Digestive and Kidney Diseases, National Institutes of Health, DHHS, Bethesda, Maryland 20892-0520, United States

## S Supporting Information

**ABSTRACT:** The molecular basis for high resistance to clinical inhibitors of HIV-1 protease (PR) was examined for the variant designated PR<sub>P51</sub> that was selected for resistance to darunavir (DRV). High resolution crystal structures of PR<sub>P51</sub> with the active site D25N mutation revealed a ligand-free form and an inhibitor-bound form showing a unique binding site and orientation for DRV. This inactivating mutation is known to increase the dimer dissociation constant and decrease DRV affinity of PR. The PR<sub>P51-D25N</sub> dimers were in the open conformation with widely separated flaps, as reported for other highly resistant variants. PR<sub>P51-D25N</sub> dimer bound two DRV molecules and showed larger separation of 8.7 Å between the closest atoms of the two flaps compared with 4.4 Å for the ligand-free structure of this mutant. The ligand-free structure, however, lacked van der Waals contacts between Ile50 and Pro81' from the other subunit in the dimer, unlike the majority of PR structures. DRV is bound inside the active site cavity; however, the inhibitor is oriented almost perpendicular to its typical position and exhibits only 2 direct hydrogen bond and two water-mediated interactions with atoms of PR<sub>P51-D25N</sub> compared with 11 hydrogen bond interactions seen for DRV bound in the typical position in wild-type enzyme. The atypical location of DRV may provide opportunities for design of novel inhibitors targeting the open conformation of PR drug-resistant mutants.



HIV-1 protease (PR) has been a successful target in AIDS therapy due to its critical role in viral maturation by hydrolyzing the Gag and Gag-Pol precursor polyproteins into mature structural and functional proteins.<sup>1,2</sup> A series of clinical HIV-1 protease inhibitors (PIs) has improved the survival of AIDS patients. One such inhibitor, darunavir (DRV), which was designed to target drug resistance by introducing strong polar interactions with the main chain atoms of the PR,<sup>3–5</sup> has been widely used for the treatment of drug-naïve patients and those infected with multidrug-resistant HIV-1.<sup>6</sup> DRV effectively inhibits PR enzymatic activity with picomolar binding affinity assessed by isothermal titration calorimetry (ITC).<sup>7</sup> However, HIV evolves resistance to DRV by selecting a combination of mutations.<sup>6</sup>

Highly DRV-resistant HIV-1 variants were selected in the laboratory to elucidate the mechanism for resistance.<sup>8</sup> A mixture of 8 highly DRV-susceptible HIV-1 clinical isolates (HIV-1<sub>MIX</sub>) containing 9–14 PI-resistant mutations was propagated in the presence of DRV. The viral population at passage 51 (HIV-1<sub>MIX</sub><sup>P51</sup>) replicated well at the concentration of 5 μM DRV, and sequencing revealed 14 amino acid substitutions in the PR gene (Figure 1).<sup>8</sup> The viral strain HIV-1<sub>MIX</sub><sup>P51</sup> was highly resistant, with half maximal effective

concentration (EC<sub>50</sub>) for inhibition of viral replication increased to more than 1 μM for DRV and most other PIs, and showed moderate resistance to saquinavir (SQV) (0.3 μM EC<sub>50</sub>).<sup>8</sup>

We have investigated the physical and biochemical properties of several resistant variants, including the HIV-1<sub>MIX</sub><sup>P51</sup> protease (PR<sub>P51</sub>).<sup>9</sup> PR<sub>P51</sub> and another highly resistant variant with 20 mutations (PR20) showed several extreme properties contributing to resistance. The affinity of DRV and SQV for PR<sub>P51</sub> as measured by isothermal titration calorimetry (ITC) gave *K<sub>L</sub>* values of 37 and 54 nM, respectively, or about 7400-fold and 135-fold weaker than the corresponding values for wild-type PR. Autocatalytic cleavage (autoprocessing) of precursor Gag-Pol polyprotein is essential to produce mature and fully active PR.<sup>10</sup> Autoprocessing of the precursor comprising the 56-amino-acid transframe region (TFR) fused to PR (TFR-PR) was inhibited the best by DRV and SQV as compared to other clinical inhibitors, although in the low micromolar range.

Received: December 2, 2013

Accepted: April 16, 2014

Published: April 16, 2014

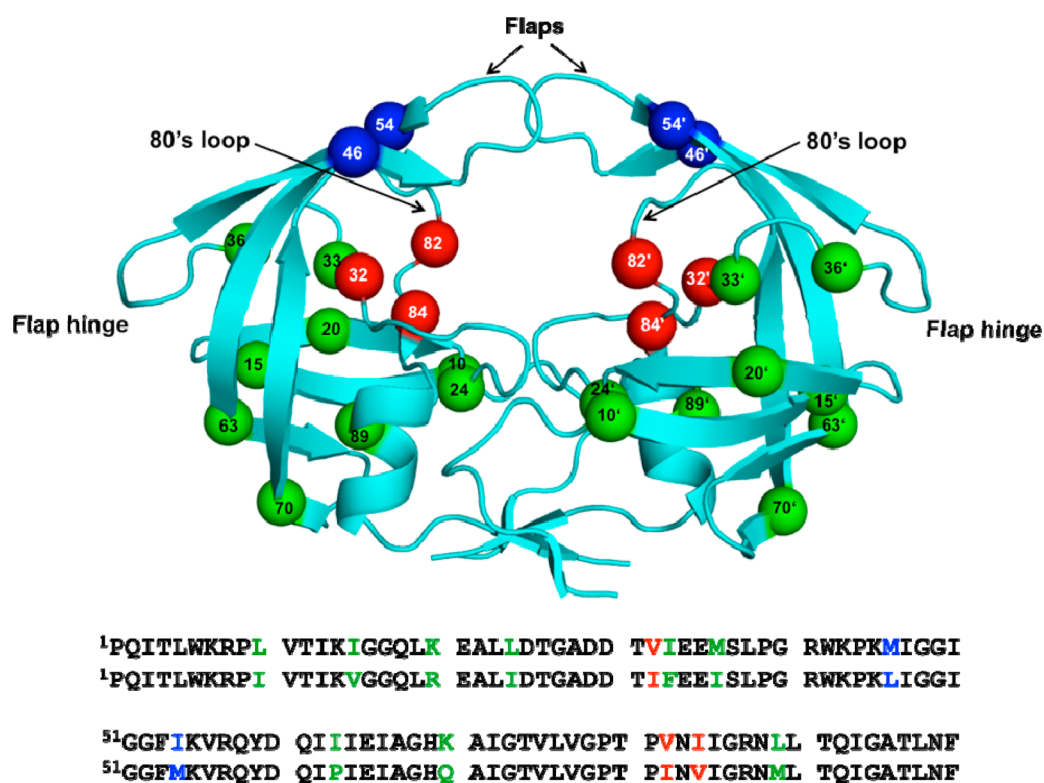


**Figure 1.** PR<sub>P51</sub> mutations. (A) Sites of the 14 drug resistant mutations mapped onto the PR<sub>P51</sub> dimer (cyan cartoon representation). The mutations located in the active site cavity are shown as red spheres, while the flap mutations are shown as blue spheres, and the mutations distal from the active site are indicated as green spheres. (B) Amino acid sequence of HIV-1 PR (upper line) and PR<sub>P51</sub> (lower line). The amino acids are colored as in panel A. Note that the wild-type PR sequence used for structural comparison includes mutations Q7K, L33I, and L63I to prevent autoproteolysis, and both proteins include C67A and C95A to eliminate potential cysteine-thiol oxidation.

However, autoprocessing of the TFR-PR<sub>P51</sub> precursor was uninhibited by DRV and marginally inhibited by SQV, at 150  $\mu$ M PI concentration.<sup>9</sup> These properties of PR<sub>P51</sub> are consistent with the high antiviral resistance to DRV measured for virus bearing this variant (>300-fold increased EC<sub>50</sub>) relative to wild-type.<sup>8</sup>

We have reported recently the structural analysis of another extremely resistant variant, PR20, which showed no inhibition of precursor autoprocessing, and  $K_L$  values for mature PR20 increased by more than 8000- and 2000-fold, respectively, for DRV and SQV.<sup>9,11</sup> Crystallographic analysis of PR20 showed fewer interactions with inhibitors and widely separated flaps in the absence of inhibitors with no contact of the flap with residues from the other subunit, unlike interactions in the corresponding structures of wild-type PR.<sup>12,13</sup> An increased separation of the flaps in the dimer may be typical of many resistant variants, as seen also for variant MDR769<sup>14</sup> and in solution studies using double electron-electron resonance (DEER) spectroscopy.<sup>15</sup>

In order to further investigate the molecular mechanisms of high-level resistance, we have determined the crystal structures of PR<sub>P51</sub> bearing the inactivating mutation D25N (PR<sub>P51-D25N</sub>) to abolish self-degradation (autoproteolysis) for sample handling during crystallization. When the D25N mutation was introduced into wild-type PR, the affinity for DRV was decreased by about 10<sup>5</sup>-fold, while no substantial changes were observed in the crystal structures.<sup>16</sup> Two structures were obtained for PR<sub>P51-D25N</sub>: a DRV-bound structure (PR<sub>P51-D25N</sub>/DRV) and a ligand-free structure (PR<sub>P51-D25N</sub>). Structural analysis revealed an unusual binding site for DRV and the

widely separated flaps that characterize the ligand-free structures of many highly resistant variants.<sup>11,14,15</sup>

## RESULTS AND DISCUSSION

**Crystal Structures of Ligand-Free and DRV-Bound PR<sub>P51-D25N</sub>.** Repeated attempts with active PR<sub>P51</sub> did not yield crystals, likely due to its enhanced autoproteolysis. Consistent with this observation even storage of the protein in 12 mM HCl prior to folding showed degradation products unlike the optimized wild-type PR. The optimized wild-type PR bears the mutations L33I and L63I shown to significantly restrict autoproteolysis of wild-type PR in addition to Q7K, which exists in PR<sub>P51</sub>.<sup>10,17</sup> Also, as DRV interactions with PR<sub>D25N</sub> are nearly identical to those in wild-type PR/DRV complex,<sup>16</sup> we resorted to using PR<sub>P51</sub> with mutation D25N for our studies.

Crystals were grown of mutant PR<sub>P51-D25N</sub> in the presence of DRV, SQV, tipranavir (TPV), and amprenavir (APV) in order to identify the structural changes associated with high level resistance. Electron density for inhibitor DRV was observed within the ligand binding cavity only in the structure of PR<sub>P51-D25N</sub>/DRV. No inhibitor was visible in the PR<sub>P51-D25N</sub> structure obtained from crystals grown in the presence of SQV, APV, or TPV, consistent with the high level resistance of this mutant. The two crystal structures designated PR<sub>P51-D25N</sub>/DRV and PR<sub>P51-D25N</sub> were refined with X-ray data at resolutions of 1.66 and 1.50 Å and R-factors of 18.9% and 15.9%, respectively. The crystallographic statistics are listed in Supplementary Table S1. PR<sub>P51-D25N</sub>/DRV was refined in space group  $P4_12_12$  with a monomer of residues numbered 1–99 in the asymmetric unit, while PR<sub>P51-D25N</sub> was refined in space group  $P4_1$  and contained

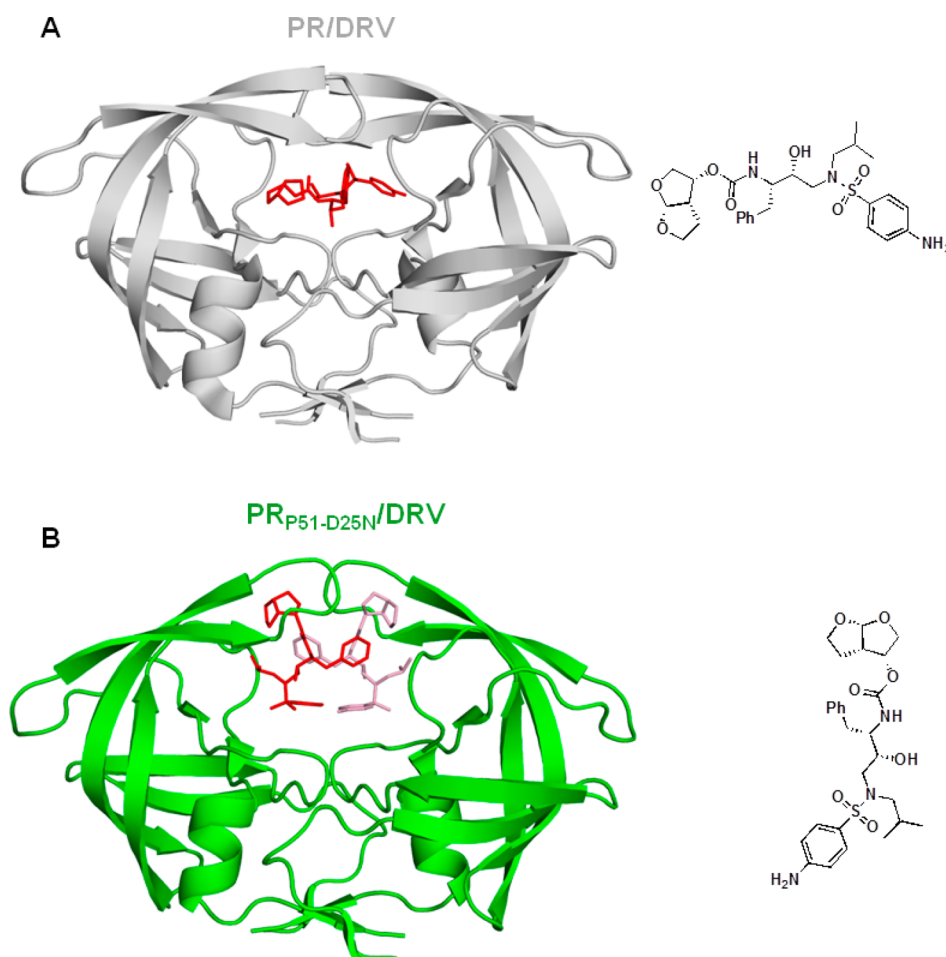


**Figure 2.** DRV binds to different sites in PR and PR<sub>P51-D25N</sub>. (A) The structure of wild-type PR (gray color) with one conformation of DRV (red sticks) (PDB ID 2IEN) bound perpendicular to the dimer interface. (B) A different position and conformation was seen for the two molecules of DRV (red sticks and pink sticks) bound symmetrically in the PR<sub>P51-D25N</sub> dimer (green color). On the right side, the chemical structure of DRV is indicated in approximately the same orientation for the two structures.

one dimer of residues numbered 1–99 and 1′–99′ in the asymmetric unit. Alternate conformations were refined for 3 residues in PR<sub>P51-D25N</sub>/DRV and 7 residues in PR<sub>P51-D25N</sub> structures. Residues 34–36 from each monomer of the two structures showed similar alternate conformations with 0.5 relative occupancy. The crystallographic dimer of PR<sub>P51-D25N</sub>/DRV was generated for structural analysis.

**PR<sub>P51-D25N</sub>/DRV Exhibits Unusual Binding Conformation of DRV.** DRV placed at the typical binding site (Figure 2A)<sup>5,18</sup> did not fit the electron density visible in the ligand binding cavity of PR<sub>P51-D25N</sub>/DRV, and thus different locations were evaluated for the inhibitor. After manual adjustment, the final monomer structure was refined with one full occupancy molecule of DRV oriented approximately perpendicular to DRV in the typical inhibitor-binding site of wild-type PR or most mutants (Figure 2B), as indicated by the clear electron density map (Figure 3A). The two molecules of DRV are related by 180° rotation and interact with each other in the binding cavity of the PR<sub>P51-D25N</sub> dimer (Figure 3B). The polar interactions between the two DRV molecules include a water-mediated hydrogen bond connecting a sulfonyl oxygen and hydroxyl group with the amino group on the aniline of the other DRV and C–H⋯water interactions with the phenyl group and the bis-THF of both DRVs. The bound DRV has

relatively few hydrogen bonds and many hydrophobic contacts with the protein (Figure 3C and D).

This DRV molecule has a different conformation and interactions from those for the regular binding mode of DRV, which has 11 direct hydrogen bond interactions and 4 water-mediated ones with PR in the wild-type PR/DRV complex (PDB ID 2IEN) (Figure 4A and 4B).<sup>5</sup> Many van der Waals contacts were observed between PR<sub>P51-D25N</sub> and DRV with distances ranging from 3.8 to 4.2 Å. In the crystal structure of PR<sub>P51-D25N</sub>/DRV, DRV forms two direct hydrogen bonds with the main chain amides of Gly49 and Gly50, and three water molecules mediate hydrogen bond interactions with Gly27, Asp30, and Gly27′ from the crystallographic dimer. van der Waals interactions occurred between DRV and PR<sub>P51-D25N</sub> residues Asn25, Ala28, Ile47, Gly48, Gly49, Ile50, Gly52, Phe53, Met54, Thr80, Pro81′, Ile82, and Val84. These interacting residues include mutations of V32I, I54M, V82I, and I84V from the selected P51 isolate and the D25N mutation. It is probable that these mutations facilitate binding of DRV to this atypical site. Introducing the single mutation D25N in the wild-type enzyme, however, does not alter the binding of DRV observed in the crystal structure.<sup>16</sup> In addition, DRV forms interactions with residues from other symmetry-related molecules of PR<sub>P51-D25N</sub> as shown in Figure 4B and Supplementary Figure S1. The DRV molecule interacts with

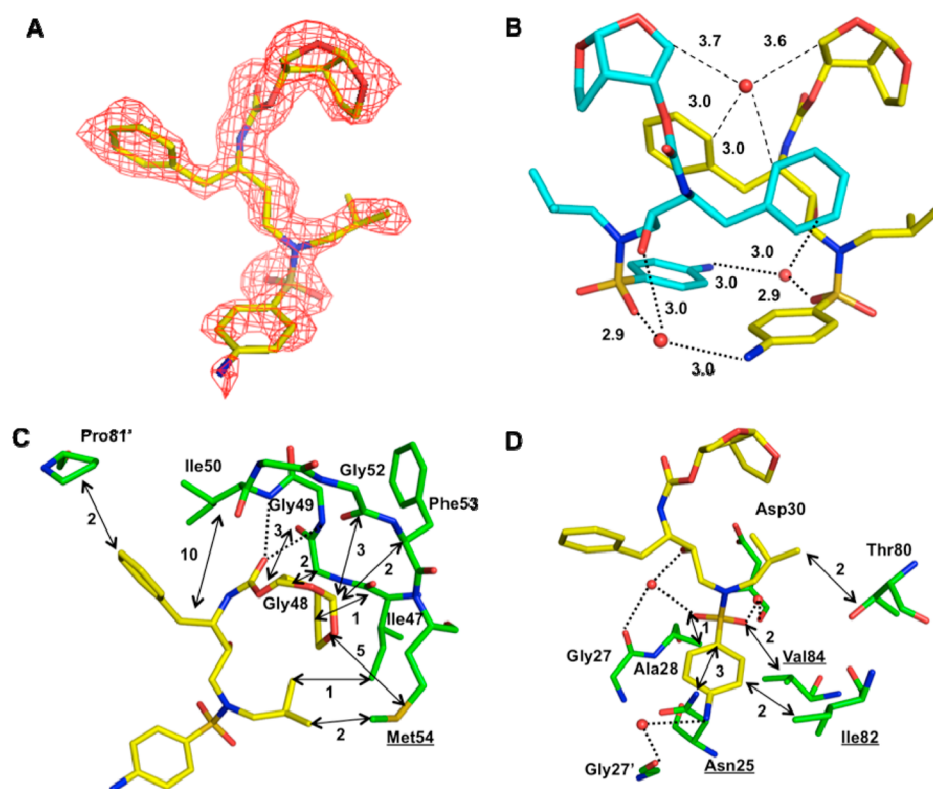


**Figure 3.** Unique binding site for DRV in PR<sub>P51-D25N</sub>. (A)  $F_o - F_c$  omit map contoured at  $2.0\sigma$  showing one molecule of DRV (yellow sticks) in the crystal structure of the monomer of PR<sub>P51-D25N</sub>/DRV. (B) Interaction between two DRV molecules in the PR<sub>P51-D25N</sub> dimer (yellow sticks and cyan sticks). Water molecules are shown as red spheres. The dotted lines represent the hydrogen bonds, and the dashed lines represent potential CH...O interactions with the interatomic distances indicated in Å. (C,D) Interactions of DRV with PR<sub>P51-D25N</sub> (green sticks). The interactions of DRV are separated into panels C and D for clarity. The interacting residues are labeled, and mutations are indicated by underlining. The dotted lines show the hydrogen bond interactions, and the double-sided arrows represent the van der Waals contacts. The number of van der Waals contacts is indicated.

Ile72 and Gln61 from two different symmetry-related monomers of PR<sub>P51-D25N</sub> (Supplementary Figure S1). The interactions include two direct hydrogen bonds between the two oxygens of the bis-THF and the amino group on the side chain of Gln61 and van der Waals contacts with Ile72 and Gln61. The existence of DRV interactions with the symmetry-related PR<sub>P51-D25N</sub> raises the possibility that crystal lattice contacts influence the atypical binding of the inhibitor.

The question of whether DRV might bind at this atypical site in wild-type enzyme can be addressed by structural comparison. The PR<sub>P51-D25N</sub>/DRV monomer shares an almost identical wide open conformation (RMSD of 0.33 Å on equivalent  $C\alpha$  atoms) with the wild-type PR crystallized with  $Mg^{2+}$  coordinated at the active site (PDB ID 2PC0).<sup>13</sup> Superposition of the two monomers reveals that three side chains of the wild-type enzyme lie close to DRV in this atypical site (Figure 5). The side chain of Ile54 in wild-type PR would hinder binding of the second THF of the bis-THF group of DRV due to short interatomic distances of 2.0–3.1 Å (Figure 5). Also, the side chains of Val82 and Ile84 in wild-type PR extend closer to the aniline group of DRV compared to the good hydrophobic contacts formed by Ile82 and Val84 in PR<sub>P51-D25N</sub>/DRV. However, rotated conformers of the side chains of Ile54, Val82, and Ile84 could allow the possible binding of DRV in the atypical site.

The affinity of DRV for binding in the typical location is expected to be decreased drastically by the mutations. The PR<sub>P51-D25N</sub> variant showed 7,400-fold lower affinity for DRV,<sup>9</sup> while introducing the single D25N mutation in the wild-type

enzyme produced about  $10^6$ -fold decreased affinity for DRV as measured by ITC with no change in the stoichiometry of binding.<sup>16</sup> Therefore, the combination of D25N plus the 14 mutations in PR<sub>P51</sub> is expected to compromise the affinity to low micromolar levels.<sup>16</sup> Consequently, DRV may favor the weaker atypical binding location observed in PR<sub>P51-D25N</sub>.

It is not the first time that DRV has been observed to bind at an unusual site in HIV-1 protease variants. A second binding site was observed in an ultrahigh resolution (0.84 Å) structure of PR<sub>V32I</sub>/DRV in addition to the typical active site binding. The second DRV bound in a groove on one flap surface where the residues Glu35', Lys45', Lys55', Val56', and Arg57' participated in the major interactions.<sup>18</sup> A similar DRV binding site occurred in the crystal structures of PR<sub>M46L</sub>/DRV and PR20/DRV.<sup>11,18</sup> Also for SQV, a second molecule was found in a location adjacent to the usual active site location in PR20/SQV and PR<sub>V32I/I47V/V82I</sub>/SQV structures.<sup>11,19</sup> Another unique binding mode was found for GB-18, specifically [3-cobalt bis(1,2-dicarbollide)]-ion, which belongs to a novel class of inorganic cobaltacarborane inhibitors, in the active site cavity of the wild-type PR (PDB ID 1ZTZ).<sup>20</sup> This binding mode involves two molecules of GB-18 positioned asymmetrically inside the pseudosymmetric active site cavity.<sup>20</sup> These binding pockets for GB-18 are formed by the residues Pro81, Ile84, and Val82 and covered by the flap residues Ile47, Gly48, and Ile54 forming a semiopen conformation of the PR dimer.<sup>20</sup> The cobaltacarborane complex was used to design novel inhibitors with linkers between two metallocarboranes to permit flexible binding to drug-resistant mutants. A similar strategy can be

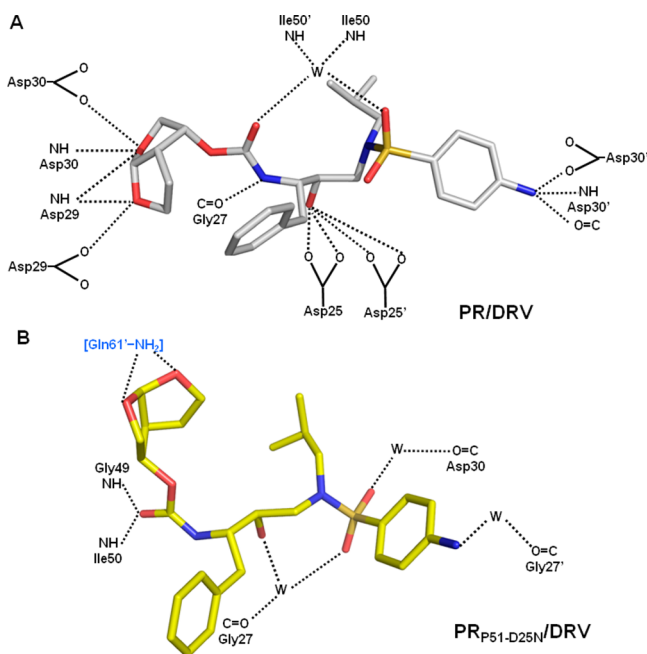


**Figure 4.** DRV has distinct hydrogen bond interactions with wild-type PR (PDB ID 2IEN) (A) and PR<sub>P51-D25N</sub> (B). DRV is represented in gray sticks and yellow sticks in PR and PR<sub>P51-D25N</sub>, respectively. The dotted lines indicate hydrogen bond interactions. Water molecules are represented by W. NH is the main chain amide group, and C=O is the main chain carbonyl group. Glu61 from a symmetry-related dimer is shown in blue within parentheses.

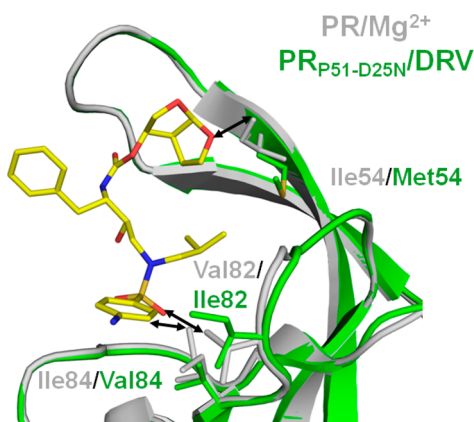


**Figure 5.** Superposition of the monomers of PR<sub>P51-D25N</sub>/DRV (green) and wild-type PR (PDB ID 2PC0) (grey). The double-headed arrows represent short interatomic contacts of 2.0–3.1 Å between DRV (yellow) and side chains of Ile54, Val82, and Ile84 in wild-type PR.

evaluated for inhibiting the open conformation dimer by chemically linking two DRV molecules as seen in the PR<sub>P51-D25N</sub>/DRV complex.

**Flaps of PR<sub>P51-D25N</sub>/DRV and PR<sub>P51-D25N</sub> Display Different Intersubunit Interactions.** Both DRV-bound and ligand-free PR<sub>P51-D25N</sub> dimers have flaps separated by a large distance between their tips. The flaps of PR<sub>P51-D25N</sub>/DRV dimer had a larger separation of 8.7 Å between the closest atoms, while the flaps were separated by 4.4 Å for PR<sub>P51-D25N</sub>. Superposition of the monomer of PR<sub>P51-D25N</sub>/DRV with each subunit of the ligand-free dimer gave the overall RMSD value of 0.97 and 0.41 Å on C $\alpha$  atoms, respectively, with large differences in the conformation of the two flaps and 80's loops (residues 79/79'

to 83/83') (Figure 6A). One of the two flaps (residues 47/47' to 54/54') of the PR<sub>P51-D25N</sub>/DRV dimer is further away from

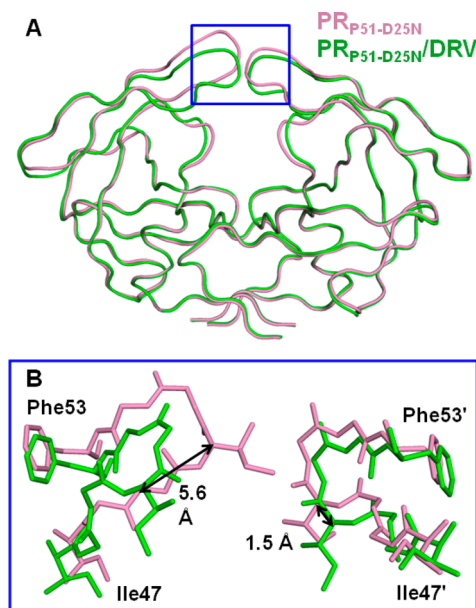


**Figure 6.** Comparison of two structures of PR<sub>P51-D25N</sub>. (A) Superposition of the overall structures of PR<sub>P51-D25N</sub> (pink) and PR<sub>P51-D25N</sub>/DRV (green). (B) The interactions of flap residues 47–54 are shown in the blue box; the numbers beside the black arrows show the distance in Å between corresponding C $\alpha$  atoms of Ile50/50' in the two structures.

the catalytic site than seen for the equivalent flap of PR<sub>P51-D25N</sub> as indicated by the distance of 5.6 Å between the equivalent C $\alpha$  atoms of Ile50 in these two structures, while the other flap conformation is more similar in the two structures with 1.5 Å distance between the C $\alpha$  atoms of Ile50' residues (Figure 6B).

The two PR<sub>P51-D25N</sub> dimer structures were compared with open conformation structures of PR and PR20 as well as their DRV-bound complexes. The open conformations of ligand-free PR20 have two unusual features relative to other reported dimer structures: widely separated flaps and no intersubunit van der Waals contacts between the flap tip and residues from the other subunit.<sup>11</sup> Therefore, the conformations were assessed by measuring the closest distance between atoms at the tip of the two flaps within one dimer structure and the closest intersubunit contact of Ile50/50' at the flap tip with Pro81'/81. The shortest interatomic distances between the flap tips were 4.0 Å in ligand-free PR<sub>P51-D25N</sub>, compared to 3.0 Å in a typical open conformation of wild-type PR (PDB ID 1HHP), 7.7 Å in another wild-type PR with Mg<sup>2+</sup> coordinated at the active site (PDB ID 2PC0), and 6.0 Å in ligand-free PR20 (PDB ID 3UF3).<sup>11–13</sup>

The various flap conformations in wild-type PR (PDB ID 1HHP), ligand-free PR<sub>P51-D25N</sub>, and ligand-free PR20 are compared in Supplementary Figure S2A. For the DRV complexes, the shortest interflap distance was 8.7 Å in PR<sub>P51-D25N</sub>/DRV compared with about 3.3 Å for typical closed conformation dimers of PR/DRV (PDB ID 2IEN) and PR20/DRV (PDB ID 3UCB) (Supplementary Figure S2B).<sup>5,11</sup> Ile50/50' at the flap tips has intersubunit van der Waals contacts of about 4.0 Å with Pro81'/81 in PR<sub>P51-D25N</sub>/DRV as observed for closed conformation inhibitor-bound dimers. The majority of dimers show intersubunit van der Waals contacts between

Ile50/50' and Pro81'/81, except for the ligand-free PR20 where these two side chains are separated by about 7 Å. In contrast, this intersubunit contact was lost in ligand-free PR<sub>P51-D25N</sub> since the closest atoms of Ile50 and Pro81' were separated by 8.5 Å. The asymmetric flap conformations of ligand-free PR<sub>P51-D25N</sub> resemble those of another open conformation dimer of PR20 (PDB ID 3UHL), which had van der Waals contact between the flap tips and asymmetric flaps with 12.2 and 5.4 Å intersubunit separation between Ile50/50' and Pro81'/81 (Figure 7). Therefore, the large separation ( $\sim 7\text{--}12$  Å) between

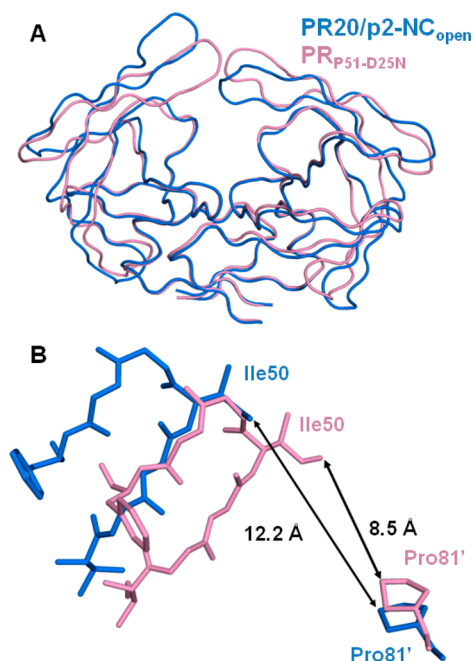


**Figure 7.** Comparison of dimers of PR<sub>P51-D25N</sub> and PR20/p2-NC<sub>open</sub> (PDB ID 3UF3). (A) Superposition of the overall structures of PR<sub>P51-D25N</sub> (pink) and PR20/p2-NC<sub>open</sub> (PDB ID 3UHL, blue). (B) The flap residues 47–53 and Pro81' of PR<sub>P51-D25N</sub> and PR20/p2-NC<sub>open</sub> are shown below. The numbers beside the black arrows show the distance in Å between Ile50 and Pro81'.

side chain atoms of Ile50 and Pro81' from the other subunit is conserved in the ligand-free dimers of the two highly resistant mutants PR20 and PR<sub>P51-D25N</sub>.

**Multiple Mutations Contribute to the Structural Changes in PR<sub>P51-D25N</sub>.** PR<sub>P51-D25N</sub> bears 14 mutations (L10I, I15V, K20R, L24I, V32I, L33F, M36I, M46L, I54M, L63P, K70Q, V82I, I84V, and L89M) as well as D25N relative to the standard wild-type PR sequence. Four mutations associated with drug resistance, V32I, M46L, V82I, and I84V, alter residues in the active site cavity where substrates and inhibitors usually bind. Additionally, “second shell” mutations L10I, L24I, L33F, and I54M alter residues that form direct interactions with residues in the active site cavity. Our crystallographic and biochemical analysis has demonstrated the changes due to the individual single mutations of L24I, V32I, M46L, I54M, and I84V, as reviewed in Weber and Agniswamy.<sup>2</sup> Several of the other substitutions in PR<sub>P51-D25N</sub> are shared by the highly resistant multiple mutant PR20, and their coordinated effects have been described previously.<sup>11</sup>

The mutations of residues V32I, V82I, and I84V in the active site cavity are assumed to contribute to the poor affinity of the PR<sub>P51</sub> mutant for inhibitors and the observed unusual binding

site for DRV in PR<sub>P51-D25N</sub> (Figure 3). The side chains of these residues form hydrophobic interactions with each other and with Val47 in all structures. Mutants PR<sub>V32I</sub> and PR<sub>I47V</sub> have altered interactions with inhibitors DRV and SQV;<sup>2,11</sup> however, V82I in the triple mutant PR<sub>V32I/I47V/V82I</sub> bearing the active site residues of HIV-2 PR does not significantly alter direct contacts with inhibitor.<sup>19</sup> Further comparison of inhibitor interactions is limited since the crystal structures of the PR<sub>P51-D25N</sub> mutant are in the open conformation without inhibitor bound in the standard active site location.

Mutations M46L and I54M alter residues in the flaps and are proposed to have small indirect effects on inhibitor binding and may alter the flap dynamics.<sup>18,21,22</sup> In PR<sub>P51-D25N</sub>/DRV, the I54M mutation introduced new van der Waals interactions with DRV (Figures 3C and 5), while M46L had no contacts with the ligand. The changes in interactions of mutated residue L24I are similar in PR<sub>P51-D25N</sub> and the single mutant PR<sub>L24I</sub>.<sup>23</sup> Ile24 gains two good van der Waals contacts with Leu90 and loses or elongates contacts (4.7 and 4.2 Å in the two subunits compared to 3.8 Å distance in wild-type PR) with Phe99' from the other subunit. Unlike the mutated side chain of L10F in PR20/DRV, in which a new hydrophobic contact was formed between the side chains of Phe10 and mutated Ile82,<sup>11</sup> mutated residue L10I in PR<sub>P51-D25N</sub> yields no new interactions with nearby residues. Mutation L33F introduces the large bulky Phe side chain, which maintains hydrophobic contacts of the wild-type enzyme, including contacts with mutated residues I15V, M36I substituting shorter side chains as reported for L33F in PR20.<sup>11</sup> Also, the flap hinge region comprising residues 34 to 43 shares a very similar conformation in PR<sub>P51-D25N</sub> and in the ligand free conformation of PR20, which is likely due to the presence of mutations M36I and I33F in both highly drug-resistant variants. The mutations in the flap hinge and flaps are likely to contribute to the extended flap conformations observed in PR<sub>P51-D25N</sub> and in inhibitor-free PR20 structures.

Mutation L89M has not been analyzed previously in structures. The side chain of Leu89 in wild-type PR forms hydrophobic contacts with the side chains of Ile64, Ile66, Ala71, Gly73, Ile85, and Asn88, as well as van der Waals and C–H...O interactions with the side chain of Thr31 (Figure 8). The mutated Met89 forms very similar contacts in PR<sub>P51-D25N</sub>, except for an additional van der Waals contact with the side chain of Val75. Mutation K20R alters a residue near the protein surface showing varied interactions with other surface side chains. Mutations L63P and K70Q also alter surface side chains that form a hydrophobic contact in the wild-type PR, which is eliminated in the mutant PR<sub>P51-D25N</sub>.

**Conclusions.** Two crystal structures were analyzed for the PR<sub>P51-D25N</sub> variant that was selected for high levels of resistance to DRV. These structures confirm the increased separation of the two flaps in the dimer and/or loss of intersubunit contacts between the flap tip and Pro81 in comparison to the open conformations seen for the ligand-free wild-type PR, as previously described for the MDR769<sup>14</sup> and PR20<sup>11</sup> highly resistant variants. Other highly resistant PR mutants have shown greater flap mobility in studies employing various techniques<sup>11,14,15,24</sup> and decreased interactions with inhibitors or substrate analogues in crystal structures.<sup>11,25,26</sup> In PR<sub>P51-D25N</sub>, however, DRV showed a unique mode of binding within the open conformation flaps and lying almost perpendicular to the typical active site position. Importantly, this new binding site for DRV may hint at designs for novel types of antiviral

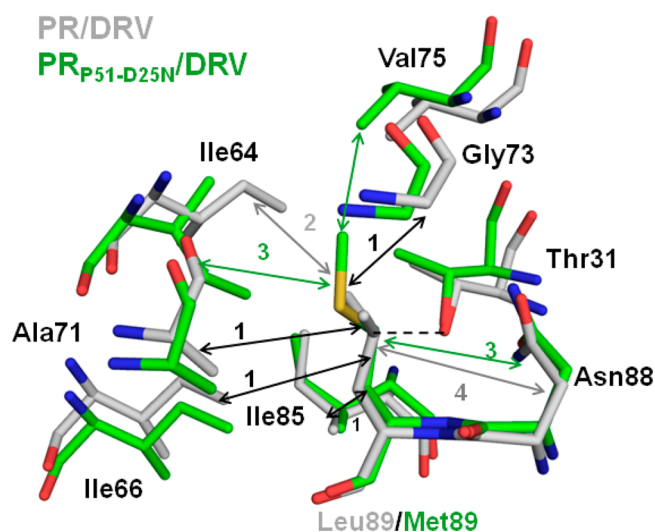


**Figure 8.** Interactions of Leu89 in PR/DRV (gray) (PDB ID 2IEN) and Met89 in PR<sub>P51-D25N</sub>/DRV (green) with neighboring residues. The double-headed arrows and the dashed lines represent the van der Waals contacts and putative C–H...O interactions, respectively, and are colored gray and green to match the structures when differences occur, while black lines indicate identical numbers of contacts in both structures. The number of van der Waals contacts is indicated by the double-headed arrows.

inhibitors that capture the open, inactive conformation of the protease.

## METHODS

**Construction, Expression, and Purification.** The HIV-1 PR from Group M (Genbank HIVHXB2CG) is designated as PR. The PR<sub>P51</sub> construct contains 14 mutations (L10I, I15V, K20R, L24I, V32I, L33F, M36I, M46L, I54M, L63P, K70Q, V82I, I84V, and L89M) plus three other mutations Q7K to minimize autoproteolysis and C67A and C95A to prevent cysteine-induced aggregation.<sup>9,10,27</sup> The mutant DNA was constructed by oligonucleotide synthesis and cloned into the pET11a vector between NdeI and BamHI restriction sites. To eliminate autoproteolysis, the inactivating mutation of D25N was introduced using the QuikChange II Site-Directed Mutagenesis Kit and confirmed by DNA sequencing. The protein was expressed in *Escherichia coli* BL21(DE3), purified and folded using the protocol described previously.<sup>28,29</sup>

**Crystallization and Data Collection.** Crystals of PR<sub>P51</sub> (including the D25N mutation) complexed with clinical inhibitors DRV and SQV were obtained by the hanging-drop vapor-diffusion method at RT using 24 well VDX plates (Hampton Research, Aliso Viejo, CA, USA). PR<sub>P51</sub> with a monomer concentration of 1.29 mg mL<sup>-1</sup> was mixed with the inhibitors at 5–10-fold molar excess. Screening Kit I solutions (Hampton Research, Aliso Viejo, CA, USA) gave good crystals of PR<sub>P51</sub> complexed with DRV (0.1 M HEPES sodium pH 7.5, 0.8 M potassium sodium tartrate tetrahydrate) and crystals of PR<sub>P51-D25N</sub> grown in the presence of SQV (0.1 M imidazole pH 6.5, 1.0 M sodium acetate trihydrate). The crystals were frozen in liquid nitrogen using 25% (v/v) glycerol as a cryoprotectant. X-ray diffraction data were collected at 100 K by remote access on the beamline BM-22 of the Southeast Regional Collaborative Access Team (SER-CAT), the Advanced Photon Source, Argonne National Laboratory, Chicago.

**Data Processing and Structure Determination.** The X-ray data were indexed, integrated, and scaled with HKL2000.<sup>30</sup> The structures were solved by molecular replacement with MOLREP in the CPP4i suite of programs<sup>31</sup> using the PR20 complex with Yb<sup>+</sup> (PDB ID 3UF3) as the starting model.<sup>11</sup> The structures were refined by REFMAC 5.2 in the CCP4 program suite 6.1.13<sup>32</sup> and refitted using COOT 0.6.1.<sup>33</sup> Alternate conformations were modeled for PR residues, inhibitors, and

solvent molecules based on the observed electron density maps. Anisotropic B factor refinement was applied for the higher resolution structure, and TLS restrained refinement was used for the lower resolution structure. Structural figures were prepared with PyMol.<sup>34</sup>

**Protein Data Bank Accession Codes.** The structure coordinates and factors have been deposited in the Protein Data Bank with access codes 4NPT for PR<sub>P51-D25N</sub>-DRV and 4NPU for PR<sub>P51-D25N</sub>.

## ASSOCIATED CONTENT

### Supporting Information

Table of crystallographic statistics and supplementary figures. This material is available free of charge via the Internet at <http://pubs.acs.org>.

## AUTHOR INFORMATION

### Corresponding Author

\*E-mail: [iweber@gsu.edu](mailto:iweber@gsu.edu).

### Present Address

<sup>†</sup>Department of Developmental Therapeutics, Fox Chase Cancer Center, Philadelphia, PA 19111.

### Notes

The authors declare no competing financial interest.

## ACKNOWLEDGMENTS

This work was supported in part by the National Institute of General Medical Sciences of the National Institutes of Health under Award Number U01GM062920 (I.T.W. and R.W.H.) and by the Georgia State University Center for Diagnostics and Therapeutics Doctoral Fellowship (Y.Z.) and by the Intramural Research Program of the NIDDK and the Intramural AIDS-Targeted Antiviral Program of the Office of the Director, NIH. The content is solely the responsibility of the authors and does not necessarily represent the official views of the National Institutes of Health. X-ray data were collected at the Southeast Regional Collaborative Access Team (SER-CAT) beamline 22BM at the Advanced Photon Source, Argonne National Laboratory. Use of the Advanced Photon Source was supported by the U.S. Department of Energy, Basic Energy Sciences, Office of Science, under Contract No. W-31-109-Eng-38. Darunavir was obtained through the NIH AIDS Research and Reference Reagent Program, Division of AIDS, NIAID, NIH.

## ABBREVIATIONS

HIV-1, human immunodeficiency virus type 1; PR<sub>P51</sub>, HIV-1 protease from group M at passage 51; PR20, mature HIV-1 protease with 20 mutations; PI, clinical inhibitor of PR; APV, ampenavir; DRV, darunavir; SQV, saquinavir; TPV, tipranavir; ITC, isothermal titration calorimetry; RMSD, root-mean-square deviation; RMSD, root-mean-square deviation

## REFERENCES

- (1) Louis, J. M., Weber, I. T., Tozser, J., Clore, G. M., and Gronenborn, A. M. (2000) HIV-1 protease: maturation, enzyme specificity, and drug resistance. *Adv. Pharmacol.* 49, 111–146.
- (2) Weber, I. T., and Agniswamy, J. (2009) HIV-1 protease: Structural perspectives on drug resistance. *Viruses* 1, 1110–1136.
- (3) Ghosh, A. K., Anderson, D. D., Weber, I. T., and Mitsuya, H. (2012) Enhancing protein backbone binding—a fruitful concept for combating drug-resistant HIV. *Angew. Chem., Int. Ed.* 51, 1778–1802.
- (4) Koh, Y., Nakata, H., Maeda, K., Ogata, H., Bilcer, G., Devasamudram, T., Kincaid, J., Boross, P., Wang, Y., and Tie, Y. (2003) Novel bis-tetrahydrofuranlyurethane-containing nonpeptidic protease inhibitor (PI) UIC-94017 (TMC114) with potent activity

against multi-PI-resistant human immunodeficiency virus in vitro. *Antimicrob. Agents Chemother.* 47, 3123–3129.

(5) Tie, Y., Boross, P. I., Wang, Y. F., Gaddis, L., Hussain, A. K., Leshchenko, S., Ghosh, A. K., Louis, J. M., Harrison, R. W., and Weber, I. T. (2004) High resolution crystal structures of HIV-1 protease with a potent non-peptide inhibitor (UIC-94017) active against multi-drug-resistant clinical strains. *J. Mol. Biol.* 338, 341–352.

(6) de Meyer, S., Vangeneugden, T., van Baelen, B., de Paepe, E., van Marck, H., Picchio, G., Lefebvre, E., and de Bethune, M. P. (2008) Resistance profile of darunavir: combined 24-week results from the POWER trials. *AIDS Res. Hum. Retroviruses* 24, 379–388.

(7) King, N., Prabu-Jeyabalan, M., Nalivaika, E., Wigerinck, P., de Bèthune, M., and Schiffer, C. (2004) Structural and thermodynamic basis for the binding of TMC114, a next-generation human immunodeficiency virus type 1 protease inhibitor. *J. Virol.* 78, 12012–12021.

(8) Koh, Y., Amano, M., Towata, T., Danish, M., Leshchenko-Yashchuk, S., Das, D., Nakayama, M., Tojo, Y., Ghosh, A. K., and Mitsuya, H. (2010) In vitro selection of highly darunavir-resistant and replication-competent HIV-1 variants by using a mixture of clinical HIV-1 isolates resistant to multiple conventional protease inhibitors. *J. Virol.* 84, 11961–11969.

(9) Louis, J. M., Aniana, A., Weber, I. T., and Sayer, J. M. (2011) Inhibition of autoprocessing of natural variants and multidrug resistant mutant precursors of HIV-1 protease by clinical inhibitors. *Proc. Natl. Acad. Sci. U.S.A.* 108, 9072–9077.

(10) Louis, J., Clore, G., and Gronenborn, A. (1999) Autoprocessing of HIV-1 protease is tightly coupled to protein folding. *Nat. Struct. Biol.* 6, 868–875.

(11) Agniswamy, J., Shen, C. H., Aniana, A., Sayer, J. M., Louis, J. M., and Weber, I. T. (2012) HIV-1 protease with 20 mutations exhibits extreme resistance to clinical inhibitors through coordinated structural rearrangements. *Biochemistry* 51, 2819–2828.

(12) Spinelli, S., Liu, Q. Z., Alzari, P. M., Hirel, P. H., and Poljak, R. J. (1991) The three-dimensional structure of the aspartyl protease from the HIV-1 isolate BRU. *Biochimie* 73, 1391–1396.

(13) Heaslet, H., Rosenfeld, R., Giffin, M., Lin, Y.-C., Tam, K., Torbett, B. E., Elder, J. H., McRee, D. E., and Stout, C. D. (2007) Conformational flexibility in the flap domains of ligand-free HIV protease. *Acta Crystallogr. D* 63, 866–875.

(14) Logsdon, B. C., Vickrey, J. F., Martin, P., Proteasa, G., Koepke, J. I., Terlecky, S. R., Wawrzak, Z., Winters, M. A., Merigan, T. C., and Kovari, L. C. (2004) Crystal structures of a multidrug-resistant human immunodeficiency virus type 1 protease reveal an expanded active-site cavity. *J. Virol.* 78, 3123–3132.

(15) de Vera, I. M., Blackburn, M. E., and Fanucci, G. E. (2012) Correlating conformational shift induction with altered inhibitor potency in a multidrug resistant HIV-1 protease variant. *Biochemistry* 51, 7813–7815.

(16) Sayer, J. M., Liu, F., Ishima, R., Weber, I. T., and Louis, J. M. (2008) Effect of the active site D25N mutation on the structure, stability, and ligand binding of the mature HIV-1 protease. *J. Biol. Chem.* 283, 13459–13470.

(17) Mildner, A. M., Rothrock, D. J., Leone, J. W., Bannow, C. A., Lull, J. M., Reardon, I. M., Sarcich, J. L., Howe, W. J., and Tomich, C.-S. C. (1994) The HIV-1 protease as enzyme and substrate: mutagenesis of autolysis sites and generation of a stable mutant with retained kinetic properties. *Biochemistry* 33, 9405–9413.

(18) Kovalevsky, A. Y., Liu, F., Leshchenko, S., Ghosh, A. K., Louis, J. M., Harrison, R. W., and Weber, I. T. (2006) Ultra-high resolution crystal structure of HIV-1 protease mutant reveals two binding sites for clinical inhibitor TMC114. *J. Mol. Biol.* 363, 161–173.

(19) Tie, Y., Wang, Y. F., Boross, P. I., Chiu, T. Y., Ghosh, A. K., Tozser, J., Louis, J. M., Harrison, R. W., and Weber, I. T. (2012) Critical differences in HIV-1 and HIV-2 protease specificity for clinical inhibitors. *Protein Sci.* 21, 339–350.

(20) Kozisek, M., Cigler, P., Lepsik, M., Fanfrlik, J., Rezacova, P., Brynda, J., Pokorna, J., Plesek, J., Gruner, B., Grantz Saskova, K., Vaclavikova, J., Kral, V., and Konvalinka, J. (2008) Inorganic

polyhedral metallocarborane inhibitors of HIV protease: a new approach to overcoming antiviral resistance. *J. Med. Chem.* 51, 4839–4843.

(21) Zhang, H., Wang, Y. F., Shen, C. H., Agniswamy, J., Rao, K. V., Xu, C. X., Ghosh, A. K., Harrison, R. W., and Weber, I. T. (2013) Novel P2 tris-tetrahydrofuran group in antiviral compound 1 (GRL-0519) fills the S2 binding pocket of selected mutants of HIV-1 protease. *J. Med. Chem.* 56, 1074–1083.

(22) Shen, C. H., Wang, Y. F., Kovalevsky, A. Y., Harrison, R. W., and Weber, I. T. (2010) Amprenavir complexes with HIV-1 protease and its drug-resistant mutants altering hydrophobic clusters. *FEBS J.* 277, 3699–3714.

(23) Liu, F., Boross, P. I., Wang, Y. F., Tozser, J., Louis, J. M., Harrison, R. W., and Weber, I. T. (2005) Kinetic, stability, and structural changes in high-resolution crystal structures of HIV-1 protease with drug-resistant mutations L24I, I50V, and G73S. *J. Mol. Biol.* 354, 789–800.

(24) Cai, Y., Yilmaz, N. K., Myint, W., Ishima, R., and Schiffer, C. A. (2012) Differential flap dynamics in wild-type and a drug resistant variant of HIV-1 protease revealed by molecular dynamics and NMR relaxation. *J. Chem. Theory Comput.* 8, 3452–3462.

(25) Liu, Z., Yedidi, R. S., Wang, Y., Dewdney, T. G., Reiter, S. J., Brunzelle, J. S., Kovari, I. A., and Kovari, L. C. (2013) Crystallographic study of multi-drug resistant HIV-1 protease lopinavir complex: mechanism of drug recognition and resistance. *Biochem. Biophys. Res. Commun.* 437, 199–204.

(26) Saskova, K. G., Kozisek, M., Rezacova, P., Brynda, J., Yashina, T., Kagan, R. M., and Konvalinka, J. (2009) Molecular characterization of clinical isolates of human immunodeficiency virus resistant to the protease inhibitor darunavir. *J. Virol.* 83, 8810–8818.

(27) Wlodawer, A., and Erickson, J. (1993) Structure-based inhibitors of HIV-1 protease. *Annu. Rev. Biochem.* 62, 543–585.

(28) Sayer, J. M., Agniswamy, J., Weber, I. T., and Louis, J. M. (2010) Autocatalytic maturation, physical/chemical properties and crystal structure of group N HIV 1 protease: Relevance to drug resistance. *Protein Sci.* 19, 2055–2072.

(29) Louis, J. M., Ishima, R., Aniana, A., and Sayer, J. M. (2009) Revealing the dimer dissociation and existence of a folded monomer of the mature HIV-2 protease. *Protein Sci.* 18, 2442–2453.

(30) Otwinowski, Z., and Minor, W. (1997) Processing of X-ray diffraction data collected in oscillation mode. *Methods Enzymol* 267, 307–326.

(31) Vagin, A., and Teplyakov, A. (1997) MOLREP: an automated program for molecular replacement. *J. Appl. Crystallogr.* 30, 1022–1025.

(32) Murshudov, G. N., Vagin, A. A., and Dodson, E. J. (1997) Refinement of macromolecular structures by the maximum-likelihood method. *Acta Crystallogr., Sect. D: Biol. Crystallogr.* 53, 240–255.

(33) Emsley, P., and Cowtan, K. (2004) Coot: model-building tools for molecular graphics. *Acta Crystallogr., Sect. D: Biol. Crystallogr.* 60, 2126–2132.

(34) DeLano, W. L. (2002) *The PyMOL Molecular Graphics System*, DeLano Scientific, San Carlos, CA.